Advances in Military Technology
Vol. 21, No. 1, 2026, pp. 277-293
ISSN 1802-2308, eISSN 2533-4123
DOI 10.3849/aimt.02007

CFD Investigation of Asymmetric Three-Dimensional Supersonic Nozzle MLN for Rocket Engine

O. Abada,[1*] A. Abada,[1] H. Kbab[1], and A. Bekhti[2]

[1] *Institute of Aeronautics and Space Studies, University of Blida, Algeria*
[2] *Center for Renewable Energies Development, CDER, Algiers, Algeria*

The manuscript was received on 22 June 2025 and was accepted
after revision for publication as an original research paper on 24 May 2026.

Abstract:

This study focuses on the design of asymmetric supersonic nozzles to improve the performance of conventional axisymmetric propulsion systems. A numerical calculation program based on the Method of Characteristics (MOC) at high temperature was developed to design three-dimensional nozzles with arbitrary exit sections. The streamlines are obtained by integrating the axisymmetric flow function, and the three-dimensional geometry is generated by tracing the exit section parameters back to the throat. Five nozzle shapes were investigated: square, circular, hexagonal, rectangular, and elliptical. CFD simulations using Ansys-Fluent were performed to validate the designs for an exit Mach number of 4.00 with air as the working fluid. The results show very good agreement with the Fortran program calculations, confirming its accuracy and highlighting the influence of exit geometry on nozzle performance.

Keywords:

CFD, supersonic nozzle, Method of Characteristics, high temperature model, minimum length nozzle, streamline, Ansys-Fluent software

1 Introduction

Supersonic nozzles play a crucial role in aerospace propulsion systems, missiles, aircraft engine exhausts, and supersonic wind tunnels. Their main function is to accelerate the flow from subsonic to supersonic speeds through successive sections: the converging part, where the flow accelerates; the throat, where the Mach number reaches unity; the diverging section, where the flow expands and accelerates to supersonic speeds; and finally the exit section, which allows efficient discharge of the high speed flow. The first studies on rocket and supersonic nozzle design were carried out by Malina [1], who used a simplified perfect gas model to determine the performance

[*] *Corresponding author: Aeronautical Sciences Laboratory, Institute of Aeronautics and Space Studies, University of Blida 1, BP 270 Blida 09000, Algeria. Phone: +213 025 43 36 36, E-mail: abadaomar1970@gmail.com. ORCID 0009-0002-7659-3554.*

of rocket engines assuming a one-dimensional conical nozzle flow. Sauer [2] later developed a calculation method for supersonic flows based on the Method of Characteristics (MOC), applied to axisymmetric configurations, while Ruptash [3] used the calorically perfect gas theory to analyze the performance of supersonic wind tunnels.

With the development of computational tools, Beckwith et al. [4] improved numerical methods for axisymmetric nozzle calculations, and Rao [5] introduced the bell-shaped nozzle geometry to improve nozzle performance compared with earlier conical designs. The extension of the MOC to 3D supersonic flows was later investigated by Coburn and Dolph [6], while Rakich [7], Chushkin [8], and Ranson et al. [9] developed numerical approaches for three-dimensional supersonic flow fields. Further developments in nozzle design were made by Sivells [10], who applied the MOC to design two-dimensional and axisymmetric supersonic nozzles. Sutton [11] later presented several nozzle configurations commonly used in aeronautics, including the Minimum Length Nozzle (MLN), which produces centered expansion and efficient supersonic flow. Argrow et al. [12] studied the performance of MLN configurations and examined the influence of the sonic line in the divergent section. The first work dealing with the design of 3D nozzles with arbitrary geometries was conducted by Haddad and Moss [13].

For several decades, most nozzle design studies were based on the perfect gas assumption, which simplifies the governing equations by considering constant thermodynamic properties. However, this assumption becomes inaccurate at high temperatures, since the specific heat Cp and the specific heat ratio γ vary with temperature, as highlighted by Anderson [14] and Peterson et al. [15]. Consequently, more recent research has incorporated advanced numerical methods and CFD simulations to analyze supersonic nozzle flows, including studies on transient nozzle operation, thrust vector control, turbulence modeling, jet noise prediction, and optimized nozzle configurations [16–20]. To improve the accuracy of nozzle design under high-temperature conditions, several researchers considered calorically imperfect gas models and the influence of stagnation temperature on supersonic nozzle performance [21–23].

In addition, methods for generating 3D nozzle contours using stream functions and internal streamlines were proposed by Abada et al. [24], although these approaches require significant computational time. In this context, the present work develops a numerical calculation program for the design of asymmetric 3D supersonic nozzles with arbitrary exit sections. Five different nozzle geometries: square, circular, hexagonal, rectangular, and elliptical are designed and analyzed. The results are validated using Computational Fluid Dynamics (CFD) simulations with Ansys-Fluent under high-temperature conditions. Air is used as the working fluid with a design exit Mach number of $M_E = 4.00$ and a stagnation temperature of $T_0 = 2\,000$ K. The results are compared with published axisymmetric Minimum Length Nozzle configurations to evaluate the influence of exit geometry on supersonic nozzle performance [20–24].

2 Supersonic Minimum Length Nozzle Theory

2.1 Design Method of the Axisymmetric Supersonic Nozzle MLN

There are many possible shapes for supersonic nozzle design, such as the Ideal Contour Nozzle (TIC) and the Thrust Optimized Parabolic (TOC) nozzle. In this study, the focus is on high-performance nozzles that provide a maximum exit Mach number with minimum weight. Particular attention is given to the centered expansion nozzle, also known as the Minimum Length Nozzle. In this configuration, the flow expansion occurs through Prandtl-Meyer waves generated at the nozzle throat with an initial angle θ, as illustrated in Fig. 1.

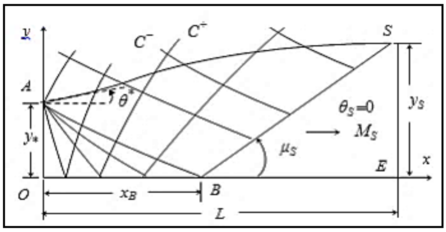

Fig. 1 Flow field in an axisymmetric nozzle MLN

Following ξ (1–3):

$$\mathrm{d}(\nu+\theta)=\frac{\sin\theta\sin\mu}{y}\mathrm{d}\xi \quad ; \quad \frac{\mathrm{d}y}{\mathrm{d}x}=\tan(\theta-\mu) \tag{1}$$

Following η (2–3):

$$\mathrm{d}(\nu-\theta)=\frac{\sin\theta\sin\mu}{y}\mathrm{d}\eta \quad ; \quad \frac{\mathrm{d}y}{\mathrm{d}x}=\tan(\theta+\mu) \tag{2}$$

where ν is the Prandtl-Meyer function at high temperature (HT).

By expressing the ξ and η directions of the Mach lines as functions of the Cartesian coordinates x and y, the governing equations of the HT MOC mathematical model can be obtained:

Following ξ (1–3):

$$\begin{cases} -\dfrac{C_p(T)}{2H(T)}\sqrt{M^2(T)-1}\mathrm{d}T+\mathrm{d}\theta=\dfrac{\sin\theta\sin\mu}{y\cos(\theta-\mu)}\mathrm{d}x \\ \dfrac{\mathrm{d}y}{\mathrm{d}x}=\tan(\theta-\mu) \end{cases} \tag{3}$$

Following η (2–3):

$$\begin{cases} -\dfrac{C_p(T)}{2H(T)}\sqrt{M^2(T)-1}\mathrm{d}T-\mathrm{d}\theta=\dfrac{\sin\theta\sin\mu}{y\sin(\theta+\mu)}\mathrm{d}x \\ \dfrac{\mathrm{d}y}{\mathrm{d}x}=\tan(\theta+\mu) \end{cases} \tag{4}$$

with $$H(T)=\int_T^{T_0}C_p(T)\mathrm{d}T\ ;\ M(T)=\frac{\sqrt{2H(T)}}{a(T)}\ ;\ a^2(T)=\gamma(T)RT\ ;\ \mu=\arcsin\frac{1}{M} \tag{5}$$

2.2 Design Method of the Three-Dimensional Asymmetric Supersonic Nozzle

The flow field in the axisymmetric Minimum Length Nozzle (MLN) is determined using a Fortran program based on the high-temperature Method of Characteristics. The 3D asymmetric nozzles with arbitrary exit sections are generated by defining streamlines in space, obtained through direct integration of the axisymmetric flow function $\psi(x, y)$ as expressed in Eq. (6) [24].

$$\frac{\partial(\rho V y\cos\theta)}{\partial x} + \frac{\partial(\rho V y\sin\theta)}{\partial y} = 0 \tag{6}$$

After transformation and substitution, the integration of Eq (6) gives:
Following ξ (1–3):

$$\psi_3 - \psi_1 = -\int_{y_1}^{y_3} \frac{\rho}{\rho_0} V y \frac{1}{M} \frac{\mathrm{d}y}{\sin(\theta - \mu)} \tag{7}$$

Following η (2–3):

$$\psi_3 - \psi_2 = \int_{y_2}^{y_3} \frac{\rho}{\rho_0} V y \frac{1}{M} \frac{\mathrm{d}y}{\sin(\theta + \mu)} \tag{8}$$

The method begins by selecting the shape of the exit section of the axisymmetric nozzle with a given length and Mach number. Different geometries can be considered, including sections with one plane of symmetry, two planes of symmetry, or no symmetry. Fig. 2 illustrates several possible exit-section shapes. The characteristic points of these shapes are then projected along the corresponding streamlines, and the surfaces formed by these streamlines define the new three-dimensional nozzle geometry.

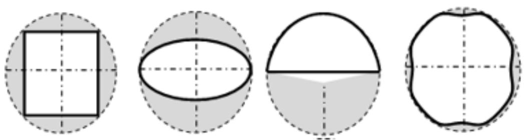

Fig. 2 Arbitrary exit section with different dispositions

3 Numerical Approach

The steady, compressible turbulent flow is governed by the following equations, which incorporate various turbulence models:

The conservation of mass is expressed as:

$$\frac{\partial\rho}{\partial t} + \frac{\partial(\rho u_i)}{\partial x_j} = 0 \tag{9}$$

The conservation of momentum equations is given by:

$$\frac{\partial(\rho u_i)}{\partial t} + \frac{\partial(\pi u_i u_j)}{\partial x_j} = \frac{\partial\left[-\left(P + \frac{2}{3}\rho k\right)\delta_{ij} + \tau_{ij}\right]}{\partial x_j} \tag{10}$$

The conservation of total energy momentum equations is given by:

$$\frac{\partial E_t}{\partial t} + \frac{\partial\left[(E_t + P)u_j\right]}{\partial x_j} = \frac{\partial q_j}{\partial x_j} + \frac{\partial(u_j\tau_{ij})}{\partial x_i} - \frac{\partial}{\partial x_j}\sum_{S=1}^{n_S} h_S J_{Sj} \tag{11}$$

3.1 Computational Domain Setup

In this research, three-dimensional axisymmetric steady-state modeling was performed to analyze the flow behavior in three-dimensional supersonic centered-expansion nozzles at different arbitrarily chosen exit sections. The simulation domain is 400Rth and 200Rth in the *x* and *y* directions, respectively, as shown in Fig. 3. The boundary conditions at the nozzle inlet or throat are: The total stagnation pressure P_0 is about 5.0 MPa and the stagnation temperature $T_0 = 2\,000$ K.

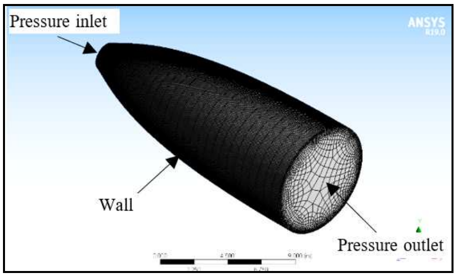

Fig. 3 Simulation domain, boundary conditions, and nozzle grid configuration

4 Results and Discussion

In this section, we present the various results obtained by our CFD numerical simulations on the Ansys-Fluent software for asymmetric three-dimensional supersonic nozzles of the centered expansion type (Minimum Length Nozzle). We begin by presenting the numerical results calculated by our Fortran calculation program to find the wall of the supersonic nozzle for a given exit Mach number and combustion chamber temperature T_0. Fig. 4 shows the shapes of the supersonic nozzles for different exit Mach numbers M_E (2.00, 3.00, 4.00 and 5.00) and stagnation temperatures T_0 (1 000 K, 2 000 K and 3 000 K). The presented figures show that the shape of the axisymmetric supersonic nozzle increases with the exit Mach number M_E and the stagnation temperature T_0.

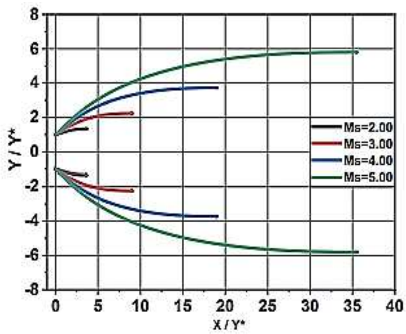

(a) Effect of the exit Mach number M_E

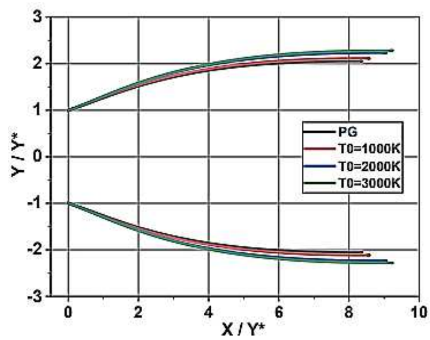

(b) Effect of the stagnation temperature T_0

Fig. 4 Design of the supersonic nozzle with cantered expansion MLN in the high-temperature model

In correspondence with the results of Fig. 4a, calculated numerically by applying the high temperature characteristic method, Tab. 1 shows the design values of MLN supersonic nozzles for different Mach numbers.

Tab. 1 Numerical values for sizing the nozzles giving the exit Mach number M_E

	$M_E = 2.00$	$M_E = 3.00$	$M_E = 4.00$	$M_E = 5.00$
L/y^*	3.6497	9.0175	19.0236	35.4889
M^*	1.2915	1.3081	1.66320	1.7671
θ^* [°]	6.2937	15.114	17.9718	21.3171
A_E/A^*	1.7711	4.9995	13.8935	33.7028
C_{Mass}	9.0569	34.695	117.457	336.1706
C_F	0.1767	0.3478	0.4440	0.4962

Fig. 5 shows the three-dimensional computational mesh and the designed geometry of the axisymmetric Minimum Length Nozzle with a circular exit section for $M_E = 4.00$ and $T_0 = 2\,000$ K. The mesh follows the nozzle contour to accurately represent the supersonic flow expansion.

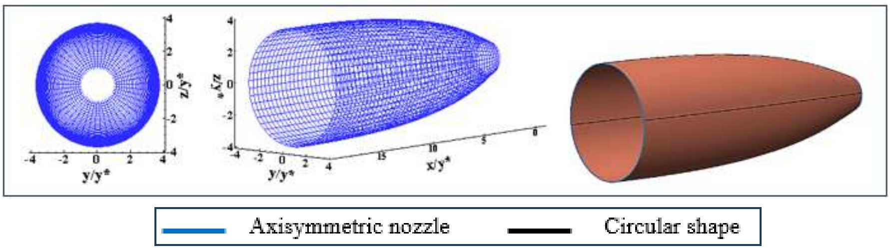

Fig. 5 Three-dimensional mesh and result design of the axisymmetric supersonic nozzle MLN with circular exit section for $T_0 = 2\,000$ K *and* $M_E = 4.00$

Fig. 6 presents the contours of Mach number, temperature ratio T/T_0, pressure ratio P/P_0, and density ratio ρ/ρ_0. These contours indicate a strong acceleration of the flow in the divergent section, while temperature, pressure, and density decrease as expected in a supersonic expansion.

Fig. 7 shows the evolution of the Mach number along the circular section of the MLN nozzle, highlighting the progressive increase of the Mach number until the design value at the exit.

Fig. 8 shows the comparison of the Mach number, temperature ratio T/T_0, pressure ratio P/P_0, and density ratio ρ/ρ_0 along the MLN nozzle wall obtained by CFD simulation using Ansys-Fluent and by the numerical Method of Characteristics (MOC). The results indicate a very good agreement between the two approaches. This confirms the accuracy of the numerical design method used for the MLN supersonic nozzle.

Tab. 2 presents the comparison between the results obtained from the numerical simulation using the MOC Fortran program and the CFD simulation using Ansys-Fluent for the circular MLN nozzle. The exit Mach number is identical in both methods ($M_E = 4.00$). Small differences are observed for the thermodynamic ratios T/T_0, P/P_0, and ρ/ρ_0, with maximum errors of about 3.95 %, 4.91 %, and 1.22 %, respectively. These small deviations confirm the good agreement and validate the accuracy of the numerical model.

Mach number contour	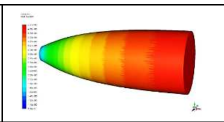	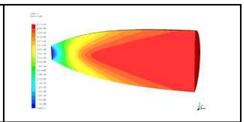
Contour of the temperature ratio T/T_0	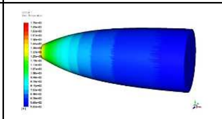	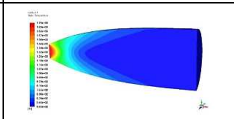
Contour of the pressure ratio P/P_0	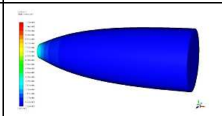	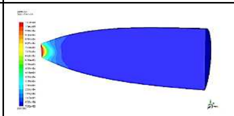
Contour of the density ratio ρ/ρ_0	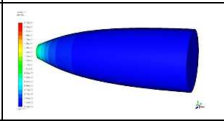	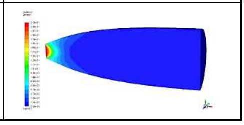

Fig. 6 Shape of the contours of the three-dimensional MLN nozzle with a circular exit section

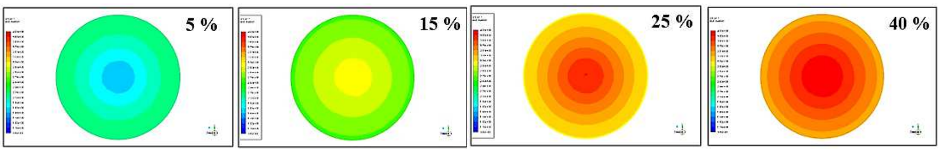

Fig. 7 Curve of the Mach number contours along the circular section MLN nozzle

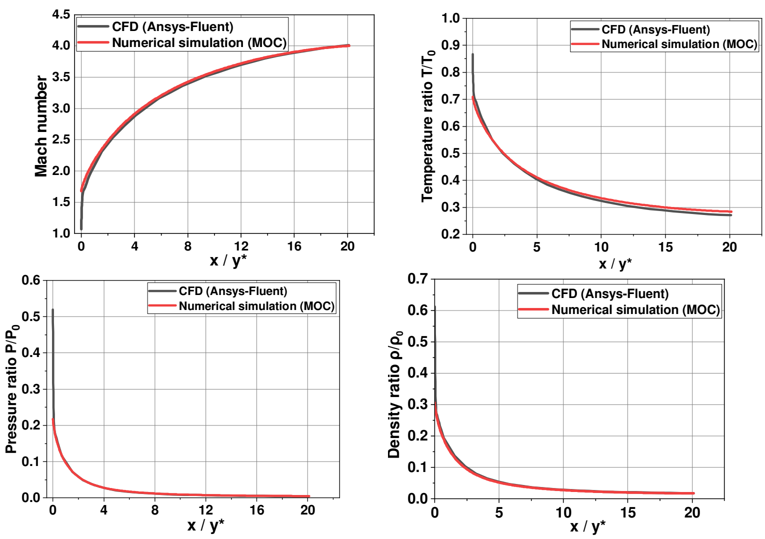

Fig. 8 Comparison of Mach number results, temperature ratio T/T_0, pressure ratio P/P_0 and density ratio ρ/ρ_0 along the MLN nozzle wall between CFD (Ansys-Fluent) and numerical simulation (MOC)

Tab. 2 Calculation of error between results by Ansys-Fluent and numerical simulation between the MLN nozzles circular shaped

	Mach	T/T_0	P/P_0	ρ/ρ_0
Numerical simulation *MOC* (Fortran)	4.00	0.28422	0.00489	0.01721
Ansys-Fluent Software simulation	4.00	0.27300	0.00465	0.01700
Error [%]	0.00	3.95	4.91	1.22

Fig. 9 shows the three-dimensional design of the supersonic nozzle with a circular exit section for $M_E = 4.00$ and $T_0 = 2\,000$ K. The geometry illustrates the expansion of the flow from the throat to the nozzle exit.

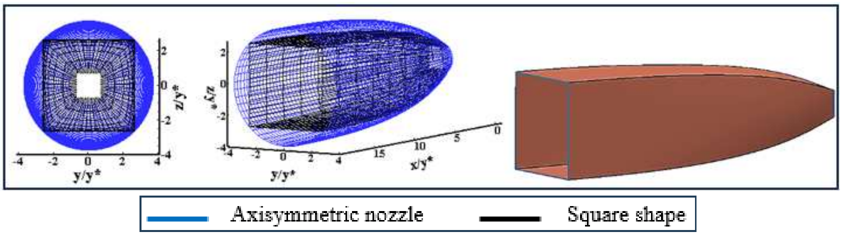

Fig. 9 Design of the supersonic nozzle with circular exit section for $M_E = 4.00$ *and* $T_0 = 2\,000$ K

Fig. 10 presents the contours of Mach number, temperature ratio T/T_0, pressure ratio P/P_0, and density ratio ρ/ρ_0, highlighting the acceleration of the flow and the corresponding decrease in thermodynamic properties along the divergent section.

Mach number contour	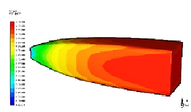	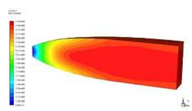
Contour of the temperature ratio T/T_0	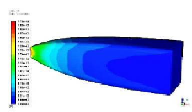	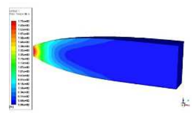
Contour of the pressure ratio P/P_0	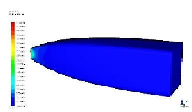	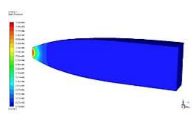
Contour of the density ratio ρ/ρ_0	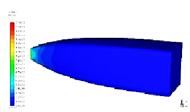	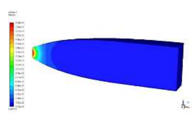

Fig. 10 Shape of the contours of the 3D MLN nozzle with a circular exit section

Fig. 11 shows the variation of the Mach number along the square section of the MLN nozzle, indicating a gradual increase of the Mach number until it reaches the design value at the exit.

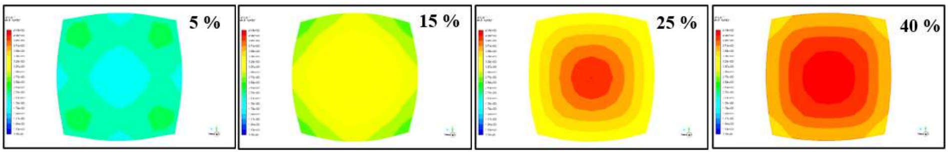

Fig. 11 Curve of the Mach number contours along the square section MLN nozzle

Fig. 12 shows the design of a supersonic nozzle with a circular exit for an exit Mach number $M_E = 4.0$ and a stagnation temperature $T_0 = 2\,000$ K. It presents the evolution of the Mach number along the nozzle, as well as the contours of temperature, pressure, and density, which gradually decrease in the divergent section as the flow accelerates.

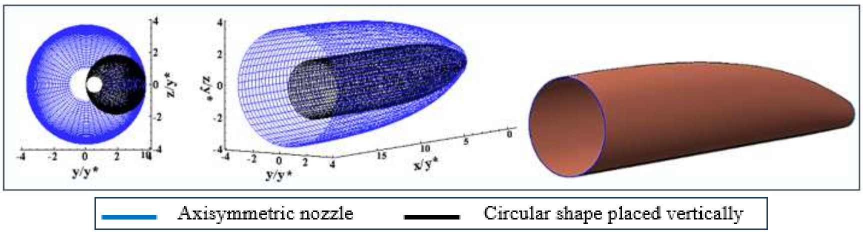

Fig. 12 Design of the supersonic nozzle with circular exit section for $M_E = 4.00$ *and* $T_0 = 2\,000$ K

On the other hand, Fig. 13 shows the three-dimensional shape of the MLN nozzle with a vertically oriented circular exit. The contours illustrate the flow distribution in space, highlighting the uniformity and symmetry of the Mach number, temperature, pressure, and density around the circular section.

Mach number contour	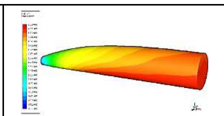	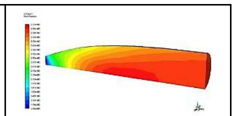
Contour of the temperature ratio T/T_0	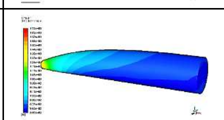	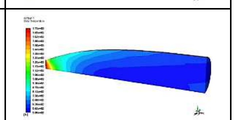
Contour of the pressure ratio P/P_0	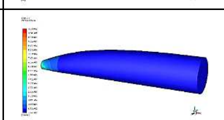	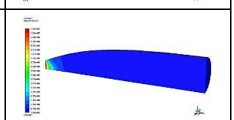
Contour of the Density ratio ρ/ρ_0	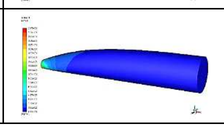	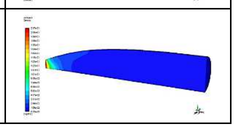

Fig. 13 Shape of the contours of the three-dimensional MLN nozzle with a circular exit section placed vertically

Finally, Fig. 14 illustrates the Mach number curves along the vertical circular section at the nozzle exit. This figure allows verification of flow regularity and confirms the attainment of the designed exit Mach number, as well as the symmetry around the nozzle's central axis.

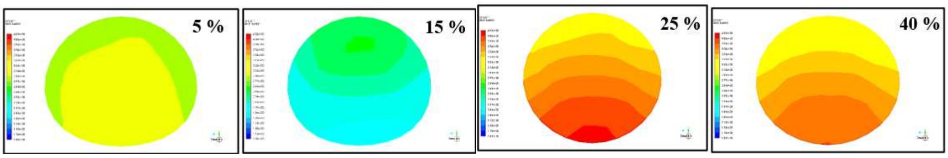

Fig. 14 Curve of the Mach number contours along the circular section placed vertically of the MLN nozzle

Fig. 15 presents the configuration of a supersonic nozzle with a circular exit section designed to reach an exit Mach number $M_E = 4.00$ at a stagnation temperature $T_0 = 2\,000$ K. The figure displays the distributions of the Mach number as well as the contours of the temperature ratio T/T_0, pressure ratio P/P_0, and density ratio ρ/ρ_0, all of which decrease progressively along the divergent part of the nozzle as the flow accelerates.

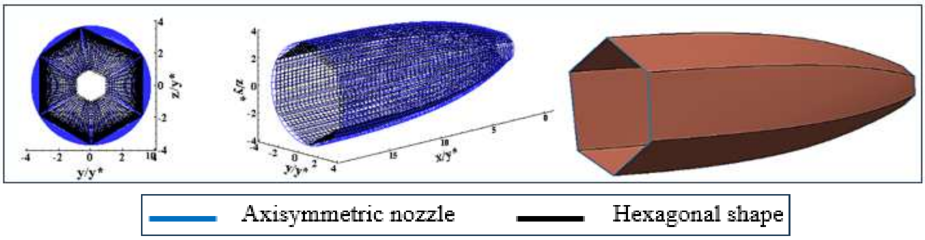

Fig. 15 Design of the supersonic nozzle with circular exit section for $M_E = 4.00$ *and* $T_0 = 2\,000$ K

In contrast, Fig. 16 depicts the contour shapes of a three-dimensional MLN nozzle equipped with a hexagonal exit section. This representation highlights the spatial distribution of the flow parameters and shows how the flow adapts to the geometric characteristics of the hexagonal outlet.

Mach number contour	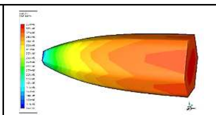	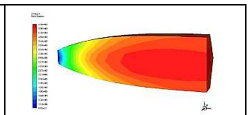
Contour of the temperature ratio T/T_0	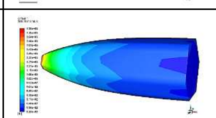	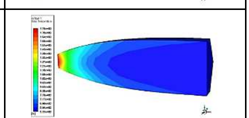
Contour of the pressure ratio P/P_0	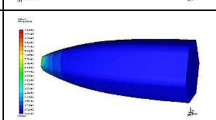	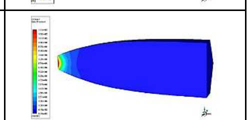
Contour of the Density ratio ρ/ρ_0	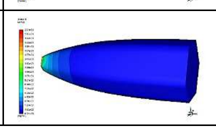	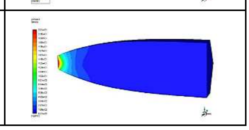

Fig. 16 Shape of the contours of the three-dimensional MLN nozzle with a hexagon exit section

Lastly, Fig. 17 illustrates the variation of the Mach number contours along the hexagonal MLN nozzle. This figure provides insight into the evolution of the Mach number across the hexagonal section and helps evaluate the uniformity of the supersonic flow at the nozzle exit.

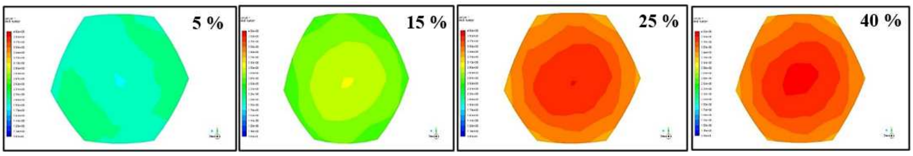

Fig. 17 Curve of the Mach number contours along the hexagonal MLN nozzle

Fig. 18 presents the design of a supersonic nozzle with a circular exit section intended to achieve an exit Mach number M_E = 4.0 with a stagnation temperature T_0 = 2 000 K. The figure displays the distributions of the Mach number together with the contours of the temperature ratio T/T_0, pressure ratio P/P_0, and density ratio ρ/ρ_0, showing their gradual variation along the divergent section as the flow accelerates.

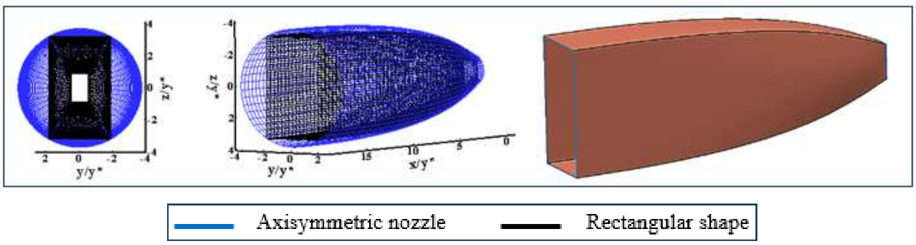

Fig. 18 Design of the supersonic nozzle with circular exit section for M_E = 4.00 *and* T_0 = 2 000 *K*

In comparison, Fig. 19 illustrates the contour shapes of the three-dimensional MLN nozzle with a rectangular exit section. This representation emphasizes the spatial arrangement of the flow field and highlights how the aerodynamic parameters adapt to the rectangular geometry at the outlet.

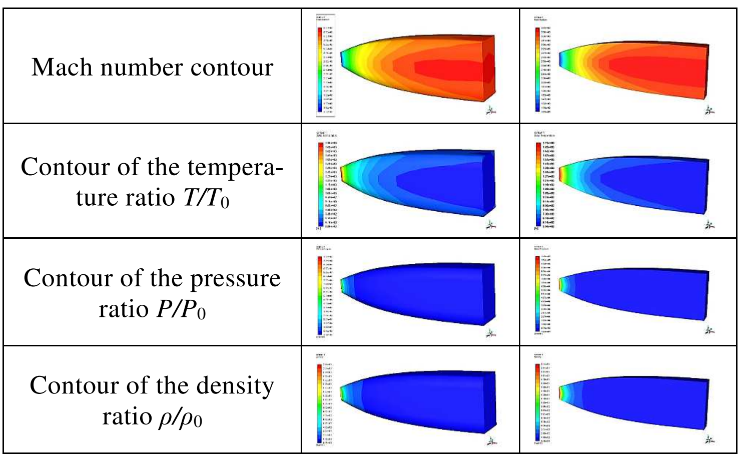

Fig. 19 Shape of the contours of the three-dimensional MLN nozzle with a rectangle exit section

Finally, Fig. 20 shows the variation of the Mach number contours along the rectangular MLN nozzle. This figure provides an overview of the Mach number evolution across the rectangular section and helps assess the distribution and uniformity of the supersonic flow at the nozzle exit.

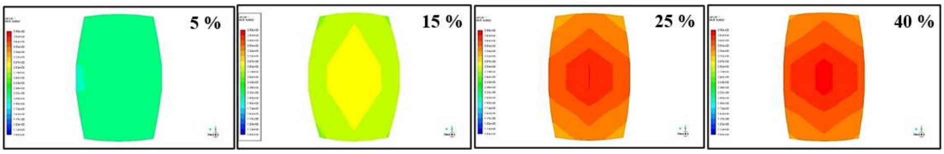

Fig. 20 Curve of the Mach number contours along the rectangle MLN nozzle

Fig. 21 presents the design of a supersonic nozzle with a circular exit section intended to achieve an exit Mach number M_E = 4.00 at a stagnation temperature T_0 = 2 000 K. The figure shows the contours of the Mach number as well as the distributions of the temperature ratio T/T_0, pressure ratio P/P_0, and density ratio ρ/ρ_0, which vary progressively along the divergent section as the flow accelerates.

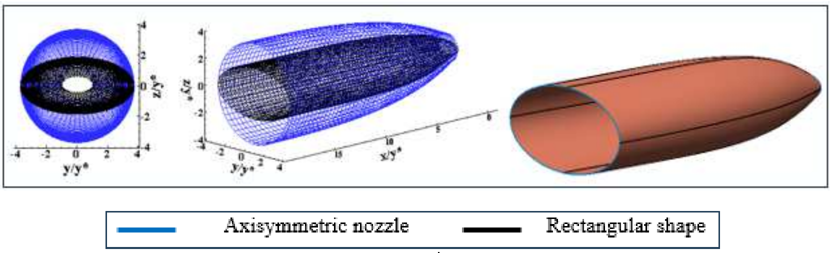

Fig. 21 Design of the supersonic nozzle with circular exit section for M_E = 4.00 *and* T_0 = 2 000 K

In contrast, Fig. 22 illustrates the contour shapes of the three-dimensional MLN nozzle with an elliptic exit section. This figure highlights the spatial distribution of the flow parameters and shows how the flow adapts to the elliptic geometry at the nozzle outlet.

Mach number contour	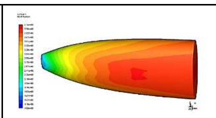	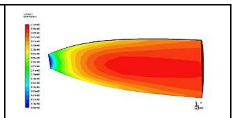
Contour of the temperature ratio T/T_0	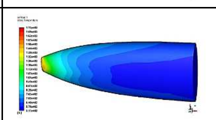	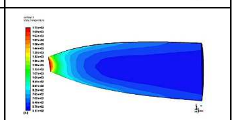
Contour of the pressure ratio P/P_0	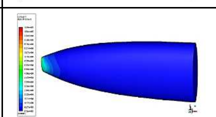	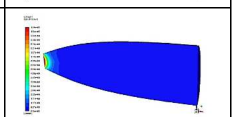
Contour of the Density ratio ρ/ρ_0	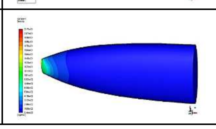	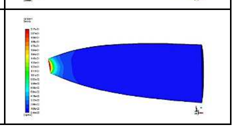

Fig. 22 Shape of contours of three-dimensional MLN nozzle with an elliptic exit section

Fig. 23 shows the variation of the Mach number contours along the elliptic MLN nozzle. It provides an overview of how the Mach number evolves along the nozzle contour and helps evaluate the uniformity of the supersonic flow at the exit.

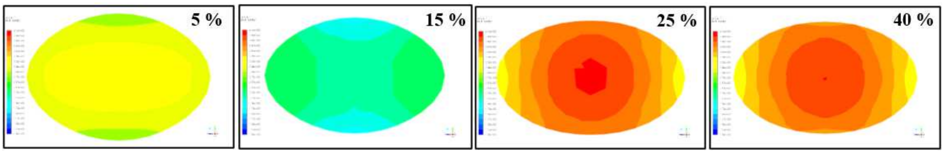

Fig. 23 Curve of the Mach number contours along the elliptic MLN nozzle

Finally, Figs 24–27 present the distributions of the main flow parameters along the contour of the three-dimensional MLN nozzles. These figures illustrate the evolution of the temperature ratio T/T_0, the Mach number, the pressure ratio P/P_0, and the density ratio ρ/ρ_0, respectively, highlighting the increase in Mach number and the corresponding decreases in temperature, pressure, and density as the flow expands through the nozzle.

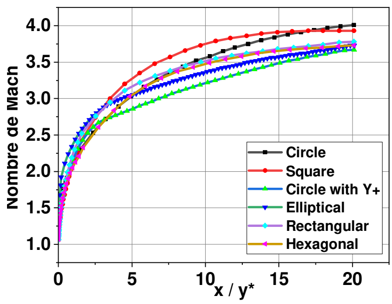

Fig. 24 Mach number along the contour of the 3D MLN nozzles

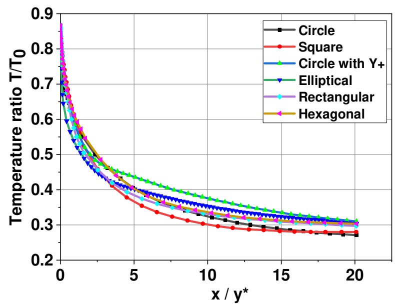

Fig. 25 Temperature ratio T/T_0 along the contour of the 3D MLN nozzles

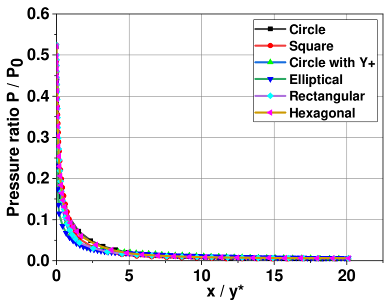

Fig. 26 Pressure ratio P/P_0 along the contour of the 3D MLN nozzles

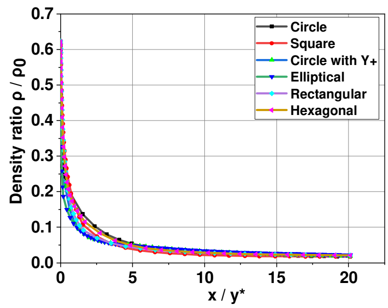

Fig. 27 Density ratio ρ/ρ_0 along the contour of 3D MLN nozzles

After analyzing the flow behavior in the three-dimensional nozzles, a comparison was made between the circular axisymmetric nozzle and the different nozzle geometries based on the results presented in Tab. 3. The analysis shows that when the circular axisymmetric nozzle reaches an exit Mach number $M_E = 4.00$, the other three-dimensional nozzle shapes produce slightly lower Mach numbers; for instance, the elliptic nozzle exhibits a decrease of about 6.75 %. Moreover, all asymmetric 3D nozzles, including those with circular sections, generate nearly the same thrust coefficient C_F. In addition, the study of the geometric variation of the centered expansion nozzle reveals that the mass coefficient C_{Mass} of the asymmetric 3D nozzles is higher than that of the circular nozzle, with an increase ranging from approximately 30 % to 54 %.

Tab. 3 Calculation of error between results of the MLN nozzles circular and different shapes

	M_E	T/T_0	P/P_0	ρ/ρ_0	C_F	C_{Mass}
Circular shape	4.00	0.273	0.00465	0.0170	0.444	117.4572
Square shape	3.93	0.280	0.00479	0.0181	0.448	165.942
Error [%]	1.75	2.50	3.004	6.077	0.890	29.22
Circular shape placed vertically	3.67	0.310	0.00560	0.0192	0.448	242.1914
Error [%]	8.25	11.94	16.964	11.46	0.890	51.50
Hexagonal shape	3.73	0.303	0.00611	0.0213	0.448	136.0062
Error [%]	6.75	9.901	23.895	20.188	0.890	13.64
Rectangular shape	3.78	0.297	0.00595	0.0212	0.448	254.5834
Error [%]	5.50	8.081	23.849	19.811	0.890	53.86
Elliptical shape	3.73	0.297	0.00595	0.0212	0.448	185.7309
Error [%]	6.75	9.901	26.772	23.423	0.890	36.76

Fig. 28 shows the Mach number contours for a supersonic nozzle at different nozzle pressure ratios (NPR). As NPR increases from 5 to 200, the flow accelerates more strongly, with the Mach number at the nozzle exit increasing and the supersonic region becoming more pronounced.

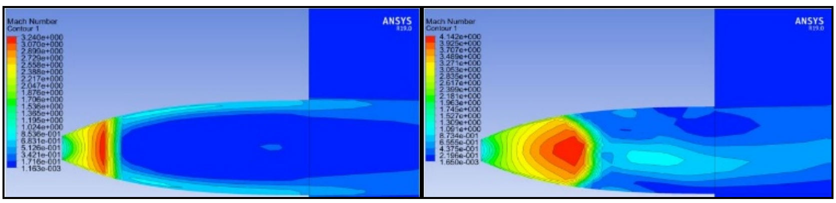

(a) *NPR* = 5 (b) *NPR* = 10

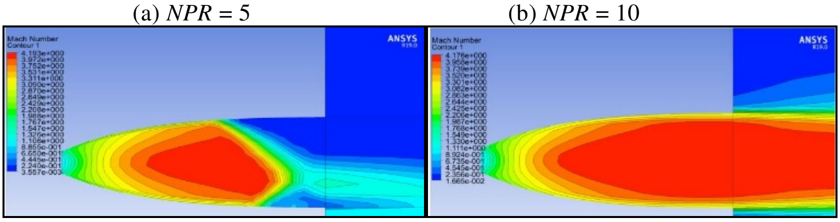

(c) *NPR* = 20 (d) *NPR* = 200

Fig. 28 Mach number contour for different values of NPR

Fig. 29 illustrates the variation of pressure along the nozzle wall as a function of *NPR*. Higher NPR values result in lower exit pressures due to stronger expansion, highlighting the influence of the pressure ratio on the flow acceleration and wall pressure distribution.

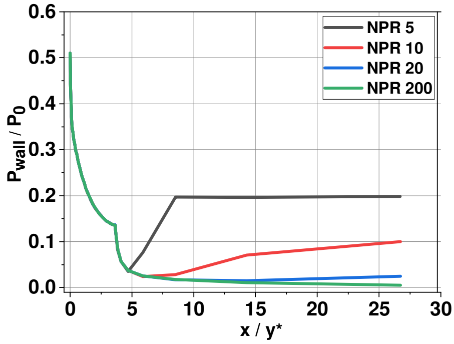

Fig. 29 Pressure variation along the wall of the nozzle as a function of NPR

5 Conclusion

This computational study investigates the impact of exit shape variation on a supersonic Minimum Length Nozzle, using CFD simulations with Ansys Fluent. Following this approach, five three-dimensional nozzles were designed and studied. Square, circular, vertically placed, hexagonal, rectangular and elliptical nozzles were used. Numerical simulations using the computational fluid dynamics (CFD) solver Ansys-Fluent were carried out to validate the design and examine the flow characteristics and performance of the three-dimensional asymmetric nozzle. Understanding these parameters is essential for the design of asymmetric supersonic nozzles to ensure their mechanical strength and safe operation in real conditions. The results of CFD numerical simulations of the different geometric shapes of minimum length nozzles have been presented in this work. The maximum difference obtained is very negligible compared to the numerical results of our Fortran calculation program. This shows the effectiveness of our program for the design of three-dimensional nozzles with arbitrary exit section. The various results obtained in this article are encouraging and show that the geometry of the nozzle exit section influences the performance of supersonic nozzles. This work could provide leads to researchers for the design of supersonic rocket nozzles.

References

[1] MALINA, F.J. Characteristics of the Rocket Motor Based on the Theory of Perfect Gases. *Journal of the Franklin Institute,* 1940, **230**(4), pp. 433-450. DOI 10.1016/ S00 16-0032(40) 91348-5.

[2] SAUER, R. *General Characteristics of the Flow Through Nozzles at Near Critical Speeds* [online]. 1947 [viewed 2025-04-09]. Available from: https://ntrs.nasa.gov/api/citations/20050019415/downloads/20050019415.pdf

[3] RUPTASH, J. *Supersonic Wind Tunnels-Theory, Design and Performance.* Toronto: University of Toronto, 1952.

[4] BECKWITH, I.E., H.W. RIDYARD and N. CROMER. *The Aerodynamic Design of High Mach Number Nozzles Utilizing Axisymmetric Flow with Application to a Nozzle of Square Test Section* [online]. 1952 [viewed 2025-04-20]. Available from: https://ntrs.nasa.gov/citations/19930083295

[5] RAO, G.V.R. Exhaust Nozzle Contour for Optimum Thrust, Marquadt Aircraft Co. *Journal of Jet Propulsion*, 1958, **28**(6), pp. 377-382. DOI 10.2514/8.7324.

[6] EVVARD, B.J.C. and S.H. MASLEN. *Three-Dimensional Supersonic Nozzles and Inlets of Arbitrary Exit Cross Section* [online]. 1952 [viewed 2025-04-10]. Available from: https://apps.dtic.mil/sti/tr/pdf/ADA380474.pdf

[7] RAKICH, J.V. Three-Dimensional Flow Calculation by the Method of Characteristics. *AIAA Journal*, 1967, **5**(10), pp. 1906-1908. DOI 10.2514/ 3.4333.

[8] CHUSHKIN, P.I. Numerical Method of Characteristics for Three-Dimensional Supersonic Flows. *Progress in Aerospace Sciences*, 1968, **9**, pp. 41-122. DOI 10.1016 / 0376-0421(68)90004-3.

[9] RANSON, V.H., H.D. THOMPSON and J.D. HOFFMAN. Three-Dimensional Supersonic Nozzle Flow Field Calculation. *Journal of Spacecraft and Rockets*, 1970, **7**(4), pp. 458-462. DOI 10.2514/3.29963.

[10] SIVELLS, J.C. *A Computer Program for the Aerodynamic Design of Axisymmetric and Planar Nozzles for Supersonic and Hypersonic Wind Tunnels* [online]. 1978 [viewed 2025-04-20]. Available from: https://apps.dtic.mil/sti/tr/pdf/ADA062944.pdf

[11] SUTTON, G.P. *Rocket Propulsion Elements*. 6th ed. Hoboken: Wiley, 1992. ISBN 0-471-52938-9.

[12] ARGROW, B.M. and G. EMANUEL. Comparison of Minimum Length Nozzles. *Journal of Fluids Engineering*, 1988, **110**(3), pp. 283-288. DOI 10.1115/1.3243546.

[13] HADDAD, A. and J.B. MOSS. Aerodynamic Design for Supersonic Nozzles of Arbitrary Cross Section. *Journal of Propulsion and Power*, 1990, **6**(6), pp. 740-746. DOI 10.2514/3.23280.

[14] ANDERSON, J.D. *Modern Compressible Flow with Historical Perspective*. 2nd ed. New York: McGraw-Hill Book Company, 1982. ISBN 0-07-001673-9.

[15] PETERSON, C.R. and P.G. HILL. *Mechanics and Thermodynamics of Propulsion*. New York: Addison-Wesley Longman, 2010. ISBN 0-13-246548-5.

[16] YU, T., X. WU, Y. YU, R. LI and H. ZHANG. Establishment and Validation of a Relationship Model Between Nozzle Experiments and CFD Results Based on Convolutional Neural Network. *Aerospace Science and Technology*, 2023, **142**, 108694. DOI 10.1016/j.ast.2023.108694.

[17] LI, D., G. WANG, J. CHENG and H. YANG. On the Thrust Vector Performance Optimization and Modeling of Supersonic Split Line Nozzles. *International Journal of Heat and Mass Transfer*, 2025, **236**, 126245. DOI 10.1016/j.ijheat masstransfer.2024. 126245.

[18] LEON-CARDONA, D., et al. Assessment of RANS Turbulence Models for the Simulation of Turbulent Compressible Flows in Convergent-Divergent Nozzles. *Chemical Engineering Transactions*, 2024, **111**, pp. 505-510. DOI 10.3303/CET24111085.

[19] HOUSMAN, J.A., G.D. STICH and C.C. KIRIS. Jet Noise Prediction using Hybrid RANS/LES with Structured Overset Grids. In: *23rd AIAA/CEAS Aeroacoustics Conference*. Denver: AIAA, 2017. DOI 10.2514/6.2017-3213.

[20] ZORE, K., C. ALIAGA, J. SELVA, L. ZORI and B. MAKAROV. High-Fidelity SBES Simulations for Supersonic Nozzle Exhaust Flows. In: *AIAA SCITECH 2024 Forum*. Orlando: AIAA, 2024. DOI 10.2514/6.2024-0753.

[21] FAN, Z., L. WANG, F. XU, X. ZHANG, B. XIE, Y. WEN, H. LI and S. AMINIAN. Influence of the Non-Equal Aligned Nozzles for Fuel Injection Inside the

Supersonic Combustion Chamber. *Scientific Reports*, 2024, **14**, 12812. DOI 10.1038/s41598-024-63544-4.

[22] ABADA, O., H. KBAB and S. HAIF. Transonic Flow Field Analysis of a Minimum Nozzle Length Rocket Engine. *Incas Bulletin*, 2024, **16**(2), pp. 3-15. DOI 10.13111/ 2066-8201.2024.16.2.1.

[23] ABADA, O., A. ABADA and A. ABDALLAH EL-HIRTSI. Effect of Bipropellant Combustion Products on the Rocket Nozzle Design. *Mechanics & Industry*, 2020, **21**, 515. DOI 10.1051/meca/2020064.

[24] ABADA, O., T. ZEBBICHE and A. ABDALLAH EL-HIRTSI. Three-Dimensional Supersonic Minimum Length Nozzle Design at High Temperature for Arbitrary Exit Cross Section. *Arabian Journal for Science and Engineering*, 2014, **39**, pp. 8233-8245. DOI 10.1007/s13369-014-1377-z.